www.cad-journal.net
Computer-Aided Design AND APPLICATIONS

A Cloud Collaborative Healthcare Platform Based on Deep Learning in The Segmentation of Maxillary Sinus

Yen-Hsun Li[1], Zheng-You Huang[2] and Yen-Kun Lin[3]

[1]National Formosa University, Yunlin, Taiwan, 900808f1@gmail.com
[2]National Formosa University, Yunlin, Taiwan, s21039785@gmail.com
[3]National Formosa University, Yunlin, Taiwan, robertlin@nfu.edu.tw

Corresponding author: Yen-Hsun Li, 900808f1@gmail.com

Abstract. This paper proposes a novel approach called ADLM++ using deep learning and active learning methods to tackle the complex training data process and achieve maxillary sinus segmentation. Prior to dental implant surgery, dentists spend lots of time diagnosing medical images due to the large variations in the shape, size, and position of the maxillary sinus among patients. The proposed method can reduce dentists' unnecessary workload and alleviate developers' required effort to prepare training data. The model can be trained with less training dataset through active learning methods and achieve better segmentation results. Then, the final training model is built as a pre-trained model and deployed in the proposed cloud collaborative healthcare platform. After dentists upload medical images, the platform automatically extracts the maxillary sinus and converts it into a 3D model, along with its volume and surface area. This information provides dentists with a visual virtual patient for accurate treatment. In the experiment, we compared the method of manual annotation by dentists with the method of segmentation using deep learning. The proposed method improves efficiency by five times and achieves a Dice Similarity Coefficient (DSC) evaluation score of 0.971±0.003. Additionally, it can improve the precision of diagnosis and surgical planning for dentists and alleviate the problem of relying on experience for diagnosis.

Keywords: deep learning, maxillary sinus, segmentation, healthcare platform
DOI: https://doi.org/10.14733/cadaps.2024.847-858

1 INTRODUCTION

According to market research statistics, the total global dental market in 2021 was 36.2 billion US dollars. In this market, the digital dental proportion is as high as 11.6% from 2012 to 2021. Additionally, the historical compound annual growth rate (CAGR) of the global digital dentistry market is 10.9%. Dental implants dominate the global digital dentistry market in 2021, accounting for 21.35% of the total revenue [1]. Clinically, the jawbone, the teeth root, the mandibular nerve canal and the maxillary sinus need to be considered before the dental treatment, especially for a dental implant procedure. Among these vital parts, the assessment of the maxillary sinus plays an important role in implant placement, sinus augmentation and orthognathic surgery. Thus, an accurate 3D segmentation of the sinus is crucial. On the other hand, an efficient image recognition is a significant foundation to affect treatment and to evaluate the surgery performance. Therefore, it is necessary and important to use deep learning technology for robust oral image recognition, measurement, 3D model reconstruction and pathological diagnosis.

Traditionally, a dental image segmentation is to recognize accurately and objectively significant regions such as the jawbone, the teeth root, the pharyngeal airway, the maxillary sinus and so on. Thresholding [2], Region Growing [3] and Active Contour [4],[5] are common methods for image segmentation. In practice, these methods are typically semi-automatic and based on the user’s experience. Recently, some deep learning methods are proposed to improve the traditional methods. For instance, O. Ronneberger [6] proposed a deep learning architecture called U-Net with contraction path and expansion path for learning and annotation from 2D medical images. After that, many researchers began to use U-Net in various fields, including bearing fault diagnosis in machines [7], building extraction and number statistics of image [8], and so on. However, it is difficult to implement in the medical image because of 3D dimension. Ö ÇİÇEK proposed 3D U-Net [9] based on U-Net [6] and improved the problem for establishing the z-axis order and orientation. After 3D U-Net was proposed, it has been widely used in the segmentation of medical images in various fields, including lung nodules [10], brain tumors [11], chest CT images [12], etc. This is a significant development for the medical field. Furthermore, F. Isensee [13] proposed nnU-Net based on a responsive framework of U-Net, 3D U-Net and U-Net Cascade, and ranked among the best in the 23 public datasets of the CHAOS (Combined (CT-MR) Healthy Abdominal Organ Segmentation) challenge, but there is no sinus segmentation in these datasets. In practice, a significant amount of time is required to annotate training datasets before the supervised deep learning. In order to address this issue, [14] developed an active learning to save a considerable amount of effort in unnecessary annotation, and has significantly improved the overall efficiency of our experimental process. Implementation of artificial intelligence in the healthcare is a compelling vision that has the potential in leading to the significant improvements for achieving the goals of providing real-time, better personalized and population medicine at lower costs [15]. Furthermore, leveraging cloud computing could execute 3D image prediction on the web to provide abundant resources and computational services [16].

In this paper, the purpose is to segment the maxillary sinus from 3D medical images for dental implant and orthognathic surgery. A customized deep learning architecture based on nnU-Net is developed to increase training efficiency with limited data and reduce annotation efforts. After completing the initial image adjustments and resampling, we employed two consecutive deep learning. The deep learnings were combined with manual modification to complete the experiment, which we refer to as ADLM++ (Active Deep Learning Method ++), the "++" indicates the use of two or more iterations. Additionally, the proposed cloud collaborative healthcare platform could be used for remote diagnosis and treatment for dentists. Finally, the accurate 3D models are not only used for the visual simulation, but also physical practices by 3D printing preoperatively.

2 MATERIALS AND METHODS

An overview of proposed platform is given in Figure 1. The first step is to collect data and then choose data without lesions as input. The second step is to do an image processing due to the insufficient memory. The third step is to obtain a training model based on the proposed ADLM++ method. At the end, the pre-trained model is integrated into the proposed cloud collaborative healthcare platform. In addition, in the whole experiment all of the annotation works were finished using 3D Slicer software (National Institutes of Health, USA) and the rest was done using Python. The study's deep learning component was implemented using the PyTorch framework. On the other hand, the 3D Slicer was used for the annotation or adjustment of annotation boundaries only. Aside from that, the complete experimental workflow and analysis were performed using Python.

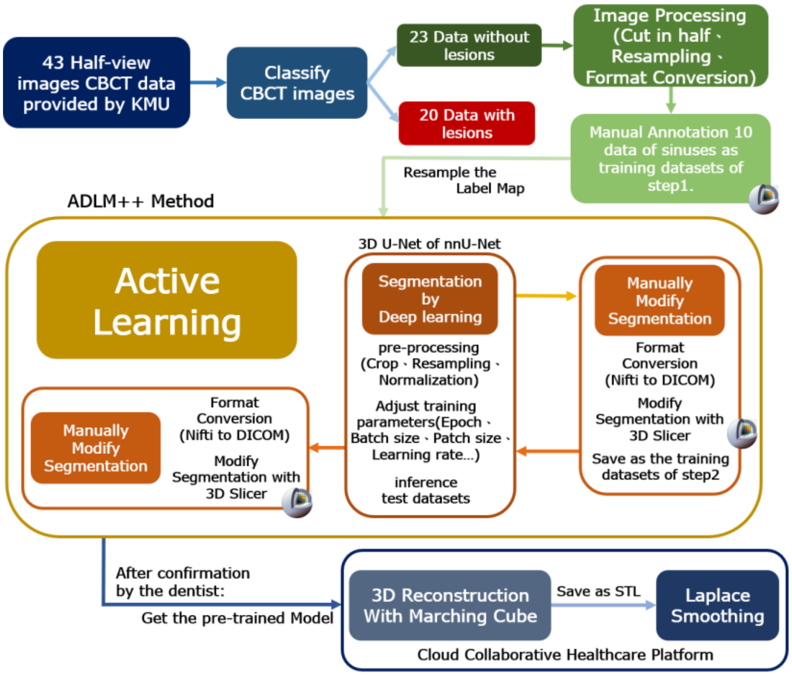

Figure 1: The overview of the proposed cloud collaborative healthcare platform.

2.1 Data Collection

We used 43 CBCT datasets (20 with lesions and 23 without lesions) from the Department of Dentistry at Kaohsiung Medical University Hospital from February to October 2022. All CBCT were acquired on the ProMax machine (Planmeca, Helsinki, Finland), with a tube voltage of 90 kV, tube current of 12 mA, and FOV of 401 * 401 mm.

2.2 Image Processing

In this paper, the training of left and right maxillary sinuses were calculated respectively because of insufficient graphic processing unit (GPU) memory during model training. Thus, we split the original CBCT images (401 * 205) into 2 sets by cropping, as shown in Figure 2.

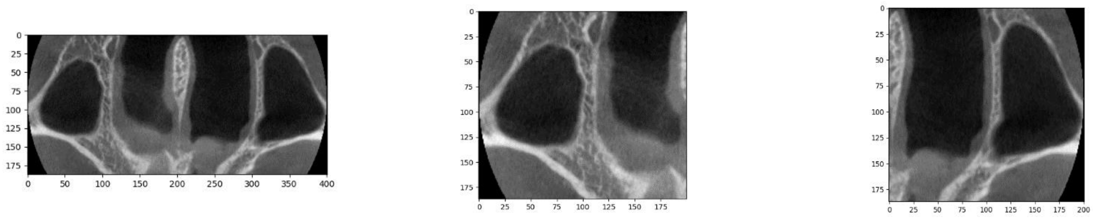

(a) (b) (c)

Figure 2: Image cropping: (a) Raw image (401*205), (b) Left half image (201*205), and (c) Right half image (200*205).

Then, all inputs were resampled to 100 x 102 pixels from 201 x 205 pixels for left sinus and 200 x 205 for right sinus. A bi-cubic interpolation method was adopted to preserve the details of the original image after shrinking, as shown in Figure 3.

(a) (b)

Figure 3: Resampling: (a) Left half image (100*102), and (b) Right half image (100*102).

2.3 Annotation

In this paper, the 23 CBCT datasets without lesions were selected as input for the training data of this study. After image processing, 10 inputs were manually annotated to establish the ground truth by 3D Slicer software. These annotated data were examined and modified by an expert with more than 3 years of experience in medical imaging, and then confirmed by another dentist with more extensive experience. In practice, the size of the patient's original CBCT was reduced from 69,950 ± 1000 KB to 1,300 ± 500 KB. The size of the annotated image was reduced from 380 ± 50 KB to 22 ± 12 KB.

2.4 ADLM++ Method

The proposed ADLM++ method includes three steps. In the first step, the first 10 inputs were used to obtain the first model after initial training. In the second step, the ground truth of the new 7 unannotated inputs was obtained by the first model and post-modified annotation for the next step. In the third step, 17 inputs (the first 10 inputs and the new 7 inputs) were adopted to calculate the second model improving the first model after the second training.

2.4.1 Deep learning method

In this paper, the deep learning architecture is based on nnU-Net in the PyTorch environment, as shown in Figure 4.

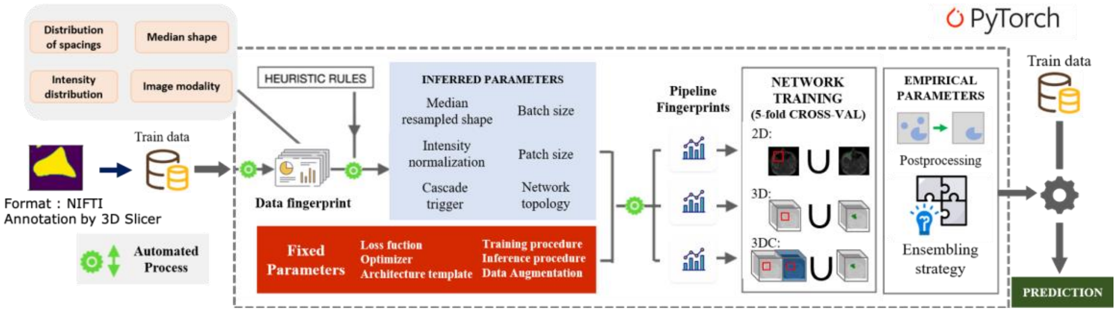

Figure 4: The configuration for deep learning-based medical image segmentation in maxillary sinus.

The primary enhancement of nnU-Net is the use of heuristic rules, which endows it with strong generalization capabilities and enables it to adapt to different tasks by providing a better hyperparameter configuration. nnU-Net includes three models that allow users to decide which one to use: 2D U-Net, suitable for general 2D single-layer images; 3D U-Net, suitable for 3D medical images; and U-Net cascade, suitable for more complex structures. For the purpose of this study, we used the 3D U-Net model in nnU-Net to segment the maxillary sinus, and the first step is to capture the data fingerprint from the training dataset. The data fingerprint of the maxillary sinus includes its image size, voxel spacing, image type, grayscale range, number of classes (here, we set the number as one) for all images, and other relevant parameters and properties.

According to these data fingerprints and hardware limitations, some significant data fingerprints are used for the image segmentation of the specific region, because they are essential and able to be formulated explicit dependencies. Additionally, it can be inferred through a set of heuristic rules for adjustment, which condense domain knowledge.

2.4.2 Active learning

In the first step, the first 10 annotated inputs consist of 9 inputs for the training, and 1 input was used for the validation. In the second step, the first model from the first step was used to obtain the segmentation of the sinus from the new 7 unannotated inputs. After that, these annotated data were examined and modified by experts. In the third step, the second model was obtained from the above 17 annotated inputs. These 17 annotated inputs include 15 inputs for the training, and 2 input was used for the validation. During these three steps, the 6 remaining inputs were adopted to test each model. In practice, the format of the prediction by deep learning method is NIfTI. Then, we convert the format into DICOM to use this result for subsequent actions [17]. After that, the post-modified annotation was conducted via the 3D Slicer. The 3D Slicer allows to superimpose the prediction results on the raw CBCT image, as shown in Figure 5.

(a) (b) (c)

Figure 5: Data conversion: (a) NIfTI data, (b) DICOM data, and (c) Use 3D Slicer to superimpose the prediction results on the raw CBCT image (the green part in image is the prediction results).

Finally, binarization was applied in the prediction results. Then, a marching cube algorithm was used on the binary image for 3D reconstruction. After 3D reconstruction, the volume and surface area could be calculated based on the discrete form of the divergence theorem [18]. In practice, the sinus models are closed surfaces. Then, a Laplacian smoothing method was applied to remove noise without excessive smoothing or distortion at the edges, as shown in Figure 6.

(a) (b)

Figure 6: 3D maxillary sinus reconstruction: (a) Original 3D model, and (d) Laplace smoothing.

2.5 Cloud Collaborative Healthcare Platform

In this study, Route53 was utilized to acquire a hospital-related domain name and manage a private domain name system (DNS) with Amazon virtual private cloud (VPC). The VPC constitutes a virtualized networking infrastructure. It facilitates the establishment of a secure and isolates environment for crucial resources, including database systems and application servers, commonly employed within academic research. Within the VPC, we employ Vue.js 2 in the Web elastic compute cloud (EC2) to render an efficient and responsive user interface. On the other hand, the application EC2 employs Django as the primary framework for handling logical operations and utilizing models.

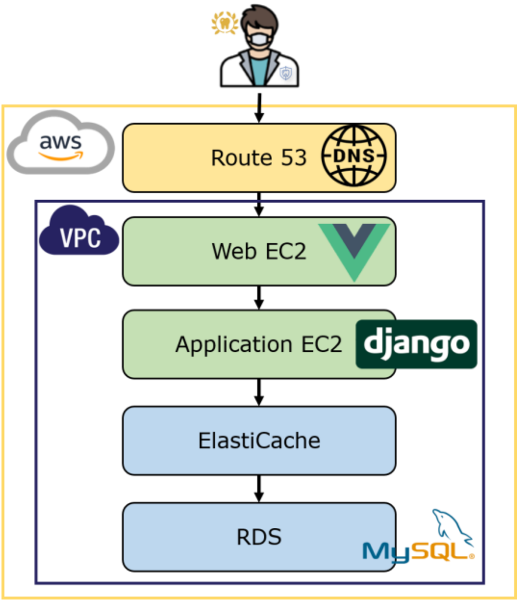

Figure 7: A cloud collaborative healthcare platform.

Furthermore, we implement caching strategies using ElastiCache to enhance the efficiency between the application and the database. Then, a relational database service (RDS) was employed to secure our databases utilizing encryption keys. In the RDS encryption, patient's data stored at rest in the underlying storage was encrypted for automated backups, read replicas, and snapshots. The architecture of the proposed platform is shown in Figure 7.

The pre-trained deep learning model in this paper was stored in the application EC2. Users account verification is required before proceeding with subsequent operations. Users create new cases by filling in the patient’s information and uploading the CBCT images. Then, the pre-trained deep learning model was used for the segmentation of the maxillary sinus. A smoothed 3D model was generated directly based on segmentation. The model could be moved, rotated, and zoomed in or out during the visualization. Users do not need to have any related knowledge of deep learning methods. They simply need to upload the CBCT, and the cloud collaborative healthcare platform will automatically generate the maxillary sinus model in few seconds. In the visualization, users could also adjust the size and transparency of the maxillary sinus model. The procedure of the proposed platform is shown in Figure 8.

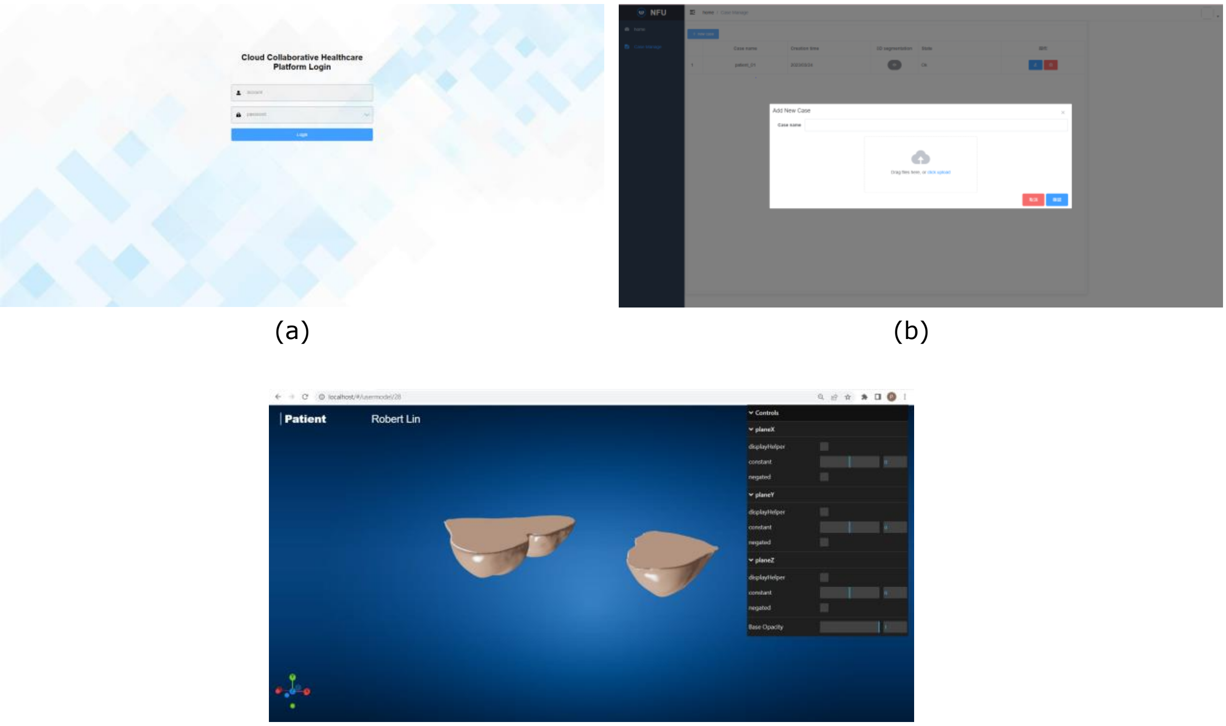

(a) (b) (c)

Figure 8: Cloud Collaborative Healthcare Platform: (a) Log in, (b) Add new case and upload data, and (c) 3D maxillary sinus visualization.

3 EXPERIMENTAL RESULTS AND DISCUSSION

The experiment for training and testing was conducted on Windows 11 with Python 3.8.5 and PyTorch 1.12.0 as a deep learning framework. The model was trained on Intel Core i9 13900K, and NVIDIA RTX 4090 GAMING X TRIO (24G).

3.1 Efficiency

The average time required for manual maxillary sinus annotation was 345.3 min(20,720s) for 10 data, it means average cost 34.5 mins(2,072s) per data, 1st deep learning assisted method was 59.1 min(3,546s), the average time for step 1 was 8.4 mins(506.5s) per data, 2nd deep learning assisted method was 38.4 min(2,304s), the average time for step 2 was 6.4 mins(384s) per data, and the final implementation of the deep learning model was able to process 6 data without any further modifications in just 12.53 seconds, resulting in an average cost of 1.253 seconds per data, e.g., Table 1.

In this paper, we employed an active learning approach to conduct two-stage deep learning training for separate segmentation of the left and right nasal sinuses. Therefore, a total of four deep learning models were trained; for each training, we set the training epoch to 1000 times, the learning rate to 1e-2, batch size to 2, and patch sizes were [163, 179, 170] and [147, 179, 161] for the left and right maxillary sinuses, respectively. In the first step of training, the left maxillary sinus took 20.11 hours. The right maxillary sinus took 17.75 hours. In the second step of training, the left maxillary sinus took 20.89 hours. The right maxillary sinus took 18.25 hours.

	Manual annotation		1st deep learning assisted manual modification		2nd deep learning assisted manual modification	
	left	right	left	right	left	right
Total times(s)	20,168	21,272	3,402	3,689	2,244	2,364
Avg times(s/1data)	2,017	2,127	486	527	374	394

Table 1: The time costing in each stage.

3.2 Accuracy

3.2.1 Quantitative analysis

In this experiment, the final training results of the left maxillary sinus are shown in Figure 9, blue line represents the training loss value, and the red line represents the verification loss value, about their loss function, we used Cross-entropy to calculate the gap, loss or error between the predicted value and the ground truth, the calculation method is as Equation (1), at the end of each epoch, an average loss value is calculated as the loss value of the training and verification, a smaller value of Cross-entropy indicates a smaller difference between the predicted and ground truth values, resulting in higher accuracy. In this experiment, to facilitate the comparison of deep learning model performance, we actually used the opposite value of the Cross-entropy, converting the value of the Cross-entropy loss function to a negative value, which makes the loss graph more intuitive to interpret. In the left maxillary sinus segmentation task, the training loss value dropped from the initial -0.1961 to -0.4896 after 1000 times of training. The green line indicates the accuracy of the model. The DSC is used as an evaluation metric, which is a measure used to compare binary image segmentation results. It calculates the degree of overlap of foreground pixels, and multiple Dice coefficients of each region are averaged to evaluate the quality of the entire image segmentation result. The calculation method is as Equation (2). In the end, the DSC of the left maxillary sinus increased from the initial 0.948 to 0.973, and the right sinus segment increased from the initial 0.935 to 0.968.

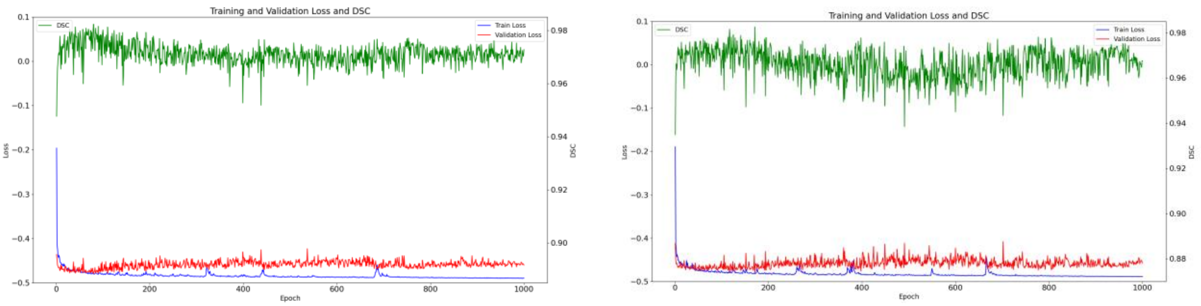

(a) (b)

Figure 9: The loss of final training model: (a) Left maxillary sinus, and (b) Right maxillary sinus.

Cross-entropy, denoted as H(p,q), is a metric used to measure the difference between the true values, p, and predicted values, q. In this experiment, "p" represents the ground truth (the data we segment manually), and "q" means the data segmented by deep learning. Then, p(i) and q(i) represent the probabilities of the sample in the distributions p and q, respectively. A smaller value of H(p,q) indicates that q is closer to the true distribution p. When q is identical to p, H(p,q) reaches the minimum value of 0. On the other hand, when q is completely different from p, H(p,q) reaches the maximum value.

$$\mathrm{H}(p,q) = -\sum p_i log_2(q_i) \quad (1)$$

In DSC, A and B are two binary images, and |A| and |B| represent the number of foreground pixels in A and B, respectively. In this case, A is the prediction result, then B is the manual annotation we did at first. |A∩B| represents the number of overlapping foreground pixels between A and B. The range of the Dice similarity coefficient is between 0 and 1, where a larger value indicates that the segmentation results of the two binary images are more similar.

$$\mathrm{DSC} = 2 \times \frac{|A \cap B|}{|A| + |B|} \quad (2)$$

Regarding the performance of the final segmentation results, as shown in Table 2, we randomly selected four patients' test data with ground truth from the first 10 cases and reconstructed the ground truth in 3D. The surface area and volume were calculated for both the ground truth and the segmentation results obtained through deep learning. Comparing the errors in surface area and volume, the volume error was approximately 6.065 ± 6.829%, while the surface area error was approximately 3.729 ± 6.149%. However, these errors fell within the acceptable range determined by the dentists, confirming that using resampled training data for model training did not affect training effectiveness. In the annotation and training process, a previous annotation approach (level set only) was used for the first four cases in Table 2. However, for the latter two cases, a new annotation method (level set with constrained intensity range) was employed. It is evident that the implementation of a modified level set method with a constrained intensity range resulted in improved accuracy. The adoption of this new labeling method enhanced the computer system's learning capabilities, leading to a significant reduction in volume error to 1.689 ± 0.88% and surface area error to 1.821 ± 1.148%.

	Case 1	Case 2	Case 3	Case 4	Case 5	Case 6
Original Volume (mm^3)	1821.356	1532.720	2046.131	2640.261	1457.432	2418.311
Original Surface (mm^2)	1017.040	890.066	1032.417	1362.642	754.115	1327.685
Segmentation Volume (mm^3)	1838.285	1606.234	2309.976	2491.334	1494.824	2437.900
Segmentation Surface (mm^2)	1023.510	905.516	1134.411	1326.295	776.490	1336.617
Volume Error (%)	0.929%	4.796%	12.895%	5.641%	2.566%	0.810%
Surface Error (%)	0.636%	1.736%	9.879%	2.667%	2.967%	0.673%

Table 2: Comparison of volume and surface area between the original and the segmentation.

3.2.2 Qualitative analysis

In Figure 10, we will use manually annotated data with ground truth to compare the segmentation results of our final training model applied directly to the original image and applied to the resampled image. Additionally, we will overlay the ground truth with the segmentation result obtained from our final training model in Figure 10(c). On the other hand, the original annotation was overlaid with the segmentation result, as shown in Figure 10(d). Some white areas from the segmentation can be observed easily around the green area from original annotation in Figure 10(d), and can see it more clearly in Figure 10(e). These white areas correspond to the segmentation result obtained directly from the original image using our final training model. It can be seen that this result is very close to the ground truth result, with a matching accuracy of over 95%. This proves that the deep learning results obtained from the training dataset after resizing can also produce similar results for the original, non-resampled images.

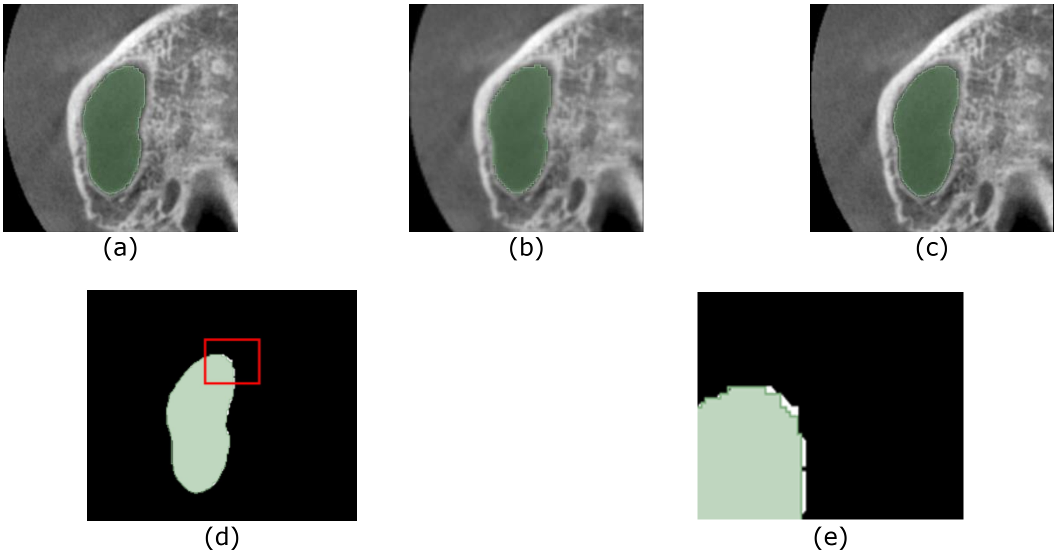

Figure 10: Comparison the original image with the resampling image and the ground truth overlay: (a) The raw image with ground truth, (b) The result of overlaying the final segmentation obtained from the resampled original image on the original image, (c) The result of using final training model for segmentation on the original-sized image and overlaying it on the original image, (d) The result of superimpose the final segmentation obtained from the original size image on the ground truth, and (e) The region of interest from the Figure 10(d) (red part).

4 CONCLUSION

In this paper, we propose an ADLM++ method based on active learning and deep learning techniques. We deployed the pre-trained model from ADLM++ on a cloud-based collaborative healthcare platform. By connecting with AWS, dentists can upload patients' medical images and obtain a comprehensive 3D sinus model on the platform. We used a limited training dataset to obtain a reliable training model, overcoming the large variations in shape, size, and position of the maxillary sinus among patients. Moreover, the efficiency increased five times compared to traditional manual annotation. Furthermore, the DSC achieved 0.971±0.003, and the errors in volume and surface area were calculated (the volume error was approximately 1.689 ± 0.88%, and the surface area error was approximately 1.821 ± 1.148%). Finally, this method can improve the precision of diagnosis and surgical planning for dentists and alleviate the problem of relying on experience for diagnosis.

5 ACKNOWLEDGMENTS

This research is funded by the National Science and Technology Council (NSTC 112-2222-E-150-001 -). We thank our colleagues from Kaohsiung Medical University School of Dentistry, who provided insight and expertise that greatly assisted the research.

Yen-Hsun Li, https://orcid.org/0009-0005-9000-8659
Zheng-You Huang, https://orcid.org/0009-0000-5667-6569
Yen-Kun Lin, https://orcid.org/0000-0002-3274-4026

REFERENCES

[1] Persistence Market Research, https://www.persistencemarketresearch.com/market-research/digital-dentistry-market.asp, Digital Dentistry Market.
[2] Wirjadi, O.: Survey of 3D image segmentation methods, Technical Report 123, Fraunhofer ITWM, Kaiserslautern, 2007, https://kluedo.ub.rptu.de/frontdoor/index/index/year/2008/docId/1978.
[3] Pohle, R.; Toennies, K. D.: Segmentation of medical images using adaptive region growing, Medical Imaging 2001: Image Processing, 4322, 2001, 1337-1346. https://doi.org/10.1117/12.431013
[4] Kass, M.; Witkin, A.; Terzopoulos, D.: Snakes: Active contour models, International journal of computer vision, 1(4), 1988, 321-331. https://doi.org/10.1007/BF00133570
[5] Derraz, F.; Beladgham, M.; Khelif, M. H.: Application of active contour models in medical image segmentation, International Conference on Information Technology: Coding and Computing, 2, 2004, 675-681. https://doi.org/10.1109/ITCC.2004.1286732
[6] Ronneberger, O.; Fischer, P.; Brox, T.: U-net: Convolutional networks for biomedical image segmentation, International Conference on Medical image computing and computer-assisted intervention, 2015, 234-241. https://doi.org/10.48550/arXiv.1505.04597
[7] Soother, D. K.; Kalwar, I. H.; Hussain, T.; Chowdhry, B. S.; Ujjan, S. M.; Memon, T. D.: A novel method based on UNET for bearing fault diagnosis. Computers, Materials and Continua, 69(1), 2021, 393-408. https://doi.org/10.32604/cmc.2021.014941
[8] Chen, D. Y.; Peng, L.; Li, W. C.; Wang, Y. D.: Building extraction and number statistics in WUI areas based on UNet structure and ensemble learning, Remote Sensing, 13(6), 2021, 1172. https://doi.org/10.3390/rs13061172
[9] Çiçek, Ö.; Abdulkadir, A.; Lienkamp, S. S.; Brox, T.; Ronneberger, O.: 3D U-Net: learning dense volumetric segmentation from sparse annotation, International conference on medical image computing and computer-assisted intervention, 2016, 424-432. https://doi.org/10.1007/978-3-319-46723-8_49
[10] Xiao, Z.; Liu, B.; Geng, L.; Zhang, F.; Liu, Y.: Segmentation of lung nodules using improved 3D-UNet neural network, Symmetry, 12(11), 2020, 1787. https://doi.org/10.3390/sym12111787
[11] Chang, J.; Zhang, X.; Ye, M.; Huang, D.; Wang, P.; Yao, C.: Brain tumor segmentation based on 3D Unet with multi-class focal loss. International Congress on Image and Signal Processing, BioMedical Engineering and Informatics, 2018, 1-5. https://ieeexplore.ieee.org/document/8633056
[12] Juarez, A. G.; Selvan, R.; Saghir, Z.; Bruijne, M. D.: A joint 3D UNet-graph neural network-based method for airway segmentation from chest CTs, In Proceedings of the International Workshop on Machine Learning in Medical Imaging, 2019, 583–591. https://doi.org/10.1007/978-3-030-32692-0_67
[13] Isensee, F.; Petersen, J.; Klein, A.; Zimmerer, D.; Jaeger, P. F.; Kohl, S.; Wasserthal, J.; K¨ohler, G.; Norajitra, T.; Wirkert, S.; Maier-Hein, K. H.: nnu-net: Self-adapting framework for u-net-based medical image segmentation, Computer Vision and Pattern Recognition, 2018. https://doi.org/10.48550/arXiv.1809.10486
[14] Jung, S. K.; Lim, H. K.; Lee, S.; Cho, Y.; Song, I. S.: Deep active learning for automatic segmentation of maxillary sinus lesions using a convolutional neural network, Diagnostics, 11(4), 2021, 688. https://doi.org/10.3390/diagnostics11040688

[15] Ahmed, Z.; Mohamed, K.; Zeeshan, S.; Dong, X.: Artificial intelligence with multi-functional machine learning platform development for better healthcare and precision medicine, Database, 2020, baaa010. https://doi.org/10.1093/database/baaa010

[16] Darwish, A.; Hassanien, A. E.; Elhoseny, M.; Sangaiah, A. K.; Muhammad, K.: The impact of the hybrid platform of internet of things and cloud computing on healthcare systems: Opportunities, challenges, and open problems, J. Ambient Intell. Hum. Comput., 10 (10) 2019, 4151-4166. https://doi.org/10.1007/s12652-017-0659-1

[17] Polzehl, J.; Tabelow, K.: Magnetic Resonance Brain Imaging: Modeling and Data Analysis Using R!. Springer, Cham. https://doi.org/10.1007/978-3-030-29184-6_3

[18] Alyassin A. M.; Lancaster J. L.; Downs J. H.; Fox P. T.: Evaluation of new algorithms for the interactive measurement of surface area and volume, Medical Physics, 21 (6), 1994, 741-752. https://doi.org/10.1118/1.597333